Hindawi
Mathematical Problems in Engineering
Volume 2022, Article ID 8304007, 19 pages
https://doi.org/10.1155/2022/8304007

Research Article

Optimization Simulation of Ultrafine Dry Powder Blow-Assisted Pipe Based on CFD

Bin Miao [1] **and Fanbao Chen** [2]

[1]*School of Resources and Geosciences, China University of Mining and Technology, Xuzhou 221116, China*
[2]*School of Safety Engineering, China University of Mining and Technology, Xuzhou 221116, China*

Correspondence should be addressed to Fanbao Chen; cfb119xz@cumt.edu.cn

Received 8 February 2022; Revised 20 February 2022; Accepted 22 February 2022; Published 14 March 2022

Academic Editor: Jiafu Su

With the increase of fire in high-rise buildings in recent years, the demand for high-performance Water Tower Fire Truck (WTFT) is increasing day by day. In order to improve the injection capacity of ultrafine dry powder of the WTFT, this article adopts the way of adding blow-assisted pipe to realize nitrogen-assisted blowing, and the internal flow field of existing blow-assisted pipe was analyzed and optimized by CFD simulation. The influence law of size parameters on the mass flow rate and velocity of ultrafine dry powder and nitrogen was analyzed and summarized under different inlet pressure conditions. The optimization result is that the diameter of the nitrogen-assisted blowing pipe is increased between 10 mm and 20 mm, the diameter of the outlet pipe is 32 mm, and the diameter of the inlet of the mixing pipe is 90 mm.

1. Introduction

With the rapid development of the economy and the acceleration of urbanization, there are more and more fires in high-rise buildings, large buildings, and chemical enterprises. This kind of building fire has the characteristics of high fire location, large fire intensity, and great difficulty in extinguishing, and its fire safety should not be underestimated [1].

Aiming at this kind of building fire, the Water Tower Fire Truck (WTFT) with the function of fire extinguishing agent injection has been paid more and more attention. It is of great significance to select a suitable fire extinguishing agent to improve the spraying height and fire extinguishing efficiency. WTFT is equipped with lifting and pressurizing jet devices, which can simultaneously fire extinguishing and fire rescue from height. In this case, a fire extinguishing agent needs to have a higher mass flow rate and velocity so that it can reach a higher height and have a good fire extinguishing effect. Halon gas extinguishing agent is the best choice when only the extinguishing effect and spraying cost are considered. However, halon extinguishing agent is harmful to the environment and has been banned for a long time [2–4]. In recent years, many scholars have studied a large number of extinguishing agents [5–11] that can replace halon. After comprehensively considering the spraying cost and extinguishing effect, ultrafine dry powder is considered as the extinguishing agent for the WTFT. Ultrafine dry powder is refined from ordinary fire extinguishing powder, with better extinguishing effectiveness [12]. Smaller particles can obtain higher flow velocity and effectively save spraying costs. However, the transport pipe of the ultrafine dry powder injection system is long, the height drop is large (usually more than 30 meters), and the diameter and direction change of the pipeline is complex, which will easily lead to the decrease of injection ability.

In order to improve the overall injection capacity of ultrafine dry powder, two schemes are considered: one is to increase the pressure of nitrogen in the ultrafine dry powder storage tank and the other is to add blow-assisted pipe. The pressure inside the dry powder storage tank is higher than that of the atmosphere. When the valve is opened, the dry powder will fill the pipe in an instant. The function of the blow-assisted pipe is to inject nitrogen into the pipe, thus

increasing the flow velocity of the ultrafine dry powder. In practical application, the former needs to improve the design value of the working pressure of the ultrafine dry powder storage tank and the compressive capacity of the official website system so that the thicknesses of the wall of the storage tank wall and transport pipe increase, resulting in an increase in the weight and cost of the whole system. The latter only needs to add a high-pressure gas source, and the cost is relatively low. Therefore, the way of adding blow-assisted pipe is chosen to improve the injection capacity of ultrafine dry powder.

Our experimental device is shown in Figure 1, which is composed of the ultrafine dry powder storage tank, high-pressure nitrogen cylinder group, injection pipeline, blow-assisted pipe, control cabinet, and ultrafine dry powder recovery device. The high-pressure nitrogen cylinder group is charged for the ultrafine dry powder storage tank. When the required pressure value is reached, the valve is opened and the ultrafine dry powder enters the injection pipeline from the storage tank. At the same time, the high-pressure nitrogen from the high-pressure nitrogen cylinder group enters the dry powder injection pipeline through the blow-assisted pipe to provide continuous power for the ultrafine dry powder flow. The ultrafine dry powder flows into the ultrafine dry powder recovery device through the pipeline and can be used in the next experiment. However, in the process of recycling, the ultrafine dry powder will absorb moisture in the air, and it is easy to cause pipe blockage after repeated tests. It takes massive manpower and financial resources to dredge the pipeline and purchase a large amount of ultrafine dry powder, so the more economical and convenient computer numerical simulation method is considered to continue the research.

Some scientists have calculated the flow of fire extinguishing agents in the tube under nitrogen pressure. For example, Elliott et al. developed a calculation program for the flow in the tube of Halon 1301 under nitrogen pressure as early as 1984 [13]. Cleary et al. compared the flow characteristics in tubes of HFC-227EA and Halon 1301, developed an experimental device that could release fire extinguishing agents constantly, and found that its flow characteristics were related to the temperature, pressure, and pipe structure of the initial extinguishing bottle [14]. Cleary et al. also compared the flow characteristics of HFC-227EA, HFC-125, and CF3I inside the pipeline and established a set of calculation programs of fire extinguishing agent steady flow under nitrogen pressure and turbulent release conditions [15]. However, few scientists have studied the flow characteristics of ultrafine dry powder in the pipeline under nitrogen pressure. Many scientists have used the CFD-DEM method to simulate and analyze dry powder at the micron level [16–22]; the simulated scenes are all dry powder inhalers with extremely small sizes. This method requires huge computational resources when simulating the large flow of dry powder in the pipeline, which is not economical.

It is hard to control single variables (pipe inlet pressure parameters and ultrafine powder mass flow rate are not constant values), and the experiment is difficult to obtain these parameters. We intend to study gas-solid two-phase flow characteristics in the pipeline under different pressure, such as mass flow rate, and flow velocity; the Eulerian model is used to simulate the flow field. Since the 21st century, with the improvement of the algorithm, the progress of the turbulence theory, and the development of the computer, the accuracy of CFD is getting higher, and it is more widely used in engineering. In the shale gas industry, erosion caused by sand particles in the pipe system was simulated by the CFD method [23]. The effects of four factors (gas velocity, sand input, particles size, and particles shape) on the erosion were simulated and analyzed in this article, and the simulation model was verified by the erosion experiment. The erosion of the blowdown valve caused by sand particles was simulated under different factors by Fluent software [24], the particle deposition under different conditions in the shale gas industry was also simulated by the CFD method, and the experiment results demonstrated the accuracy of the method [25]. CFD simulation analysis can avoid the ultrafine dry powder dampness caused by repeated experiments, strictly control the single variables, and obtain the flow characteristics of the mixed flow field in the pipeline more conveniently, which could provide a reference for the subsequent injection scheme design.

This article is mainly divided into five parts: introduction, method, mesh independence study and experimental verification, results and discussion, and conclusion. In the method part, the steps, models, and boundary conditions of the simulation are introduced. In the mesh independence study and experimental verification part, the rationality of the mesh and the reference of the calculation are proved. In the result and discussion part, the influence of each parameter on the calculation results is analyzed and discussed. This article provides a new economical way to increase the dry powder flow rate, which is of great significance in the rapid transportation of dry powder in the pipeline, the effect of dry powder injection, and the efficiency of fire extinguishing.

2. Methods

The main assumptions of this article are as follows:

(1) The flow of ultrafine dry powder and nitrogen in the pipeline is incompressible.

(2) The pipe wall is a nonsliding wall.

2.1. Geometric Models and Computational Grids. Considering the computational cost brought by simulating the whole pipeline, the blow-assisted pipe is simulated in this article. The geometric size of the blow-assisted pipe is shown in Figure 2, and its three-dimensional model of the flow field is shown in Figure 3. The geometric model was divided into unstructured grids, as shown in Figure 4.

2.2. Eulerian Model. The Eulerian model used in Fluent could be used to simulate multiple separate but interacting phases, which can be any combination of liquid, gas, or solid. The multiphase flow described in this article is a gas-solid

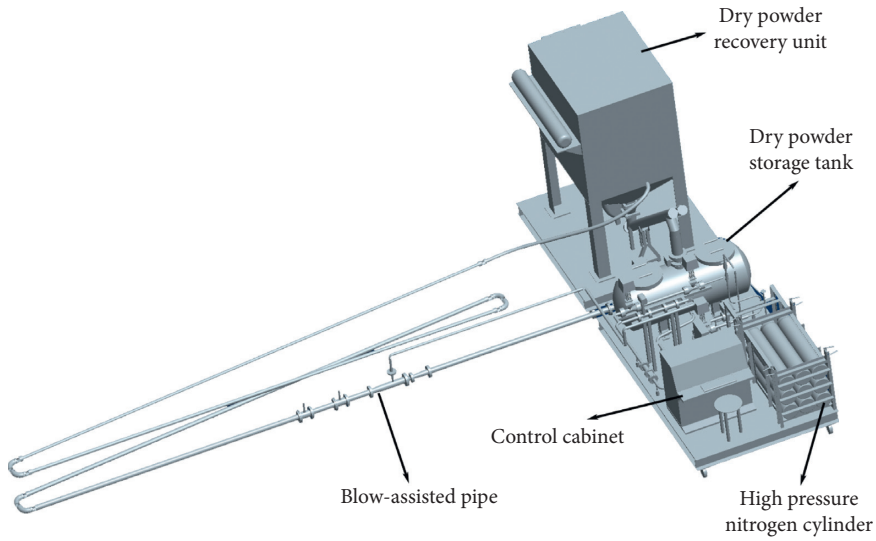

Figure 1: Ultrafine dry powder injection test equipment.

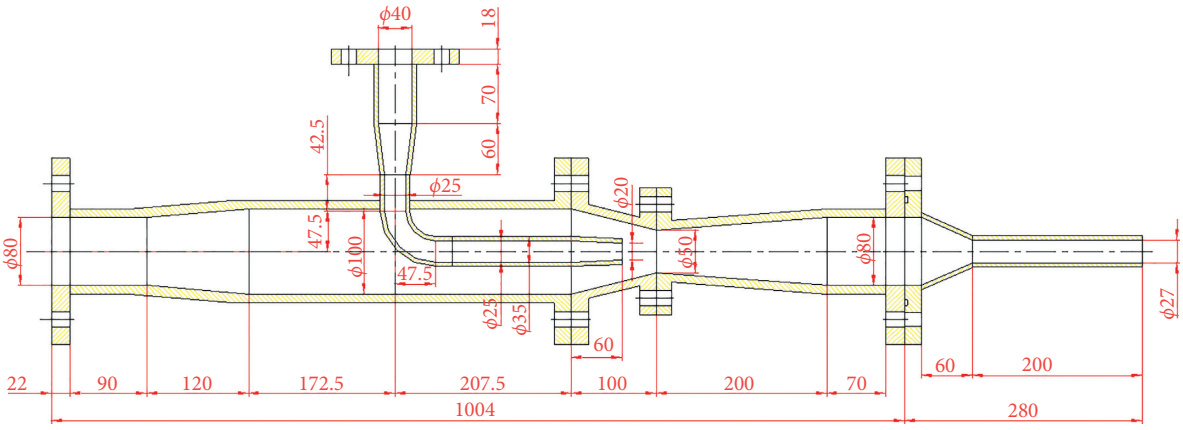

Figure 2: The size of blow-assisted pipe.

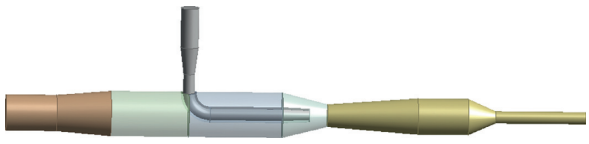

Figure 3: Three-dimensional model of flow field of blow-assisted pipe.

two-phase flow. In this study, only nitrogen and dry powder are mixed and the two phases interact with each other, so the Eulerian model is suitable for the simulation in this case. The Eulerian model is mainly used to solve the following equations.

2.2.1. Volume Fraction Equation. The volume of the q^{st} phase satisfies

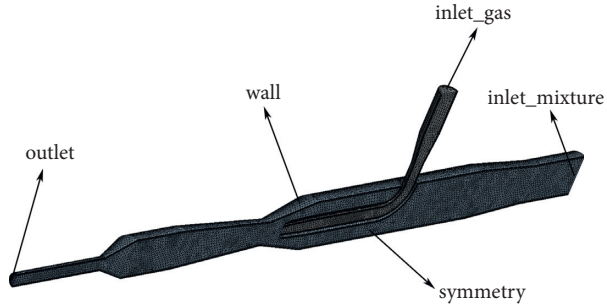

Figure 4: The mesh of blow-assisted pipe.

$$V_q = \int_V \alpha_q dV, \tag{1}$$

where

$$\sum_{q=1}^{n} \alpha_q = 1. \tag{2}$$

The effective density of the q^{st} phase can be expressed as

$$\widehat{\rho}_q = \alpha_q \rho_q, \tag{3}$$

where ρ_q is the physical density of the q^{st} phase.

2.2.2. Equation of Continuity. The volume fraction of each phase satisfies the continuity equation:

$$\frac{1}{\rho_{rq}}\left(\frac{\partial}{\partial t}\left(\alpha_q \rho_q\right) + \nabla \cdot \left(\alpha_q \rho_q \overrightarrow{v}_q\right) = \sum_{p=1}^{n}\left(\dot{m}_{pq} - \dot{m}_{qp}\right)\right), \tag{4}$$

where ρ_{rq} is the phase reference density, that is, the average volume density of the q^{st} phase.

2.2.3. Momentum Equation. For the gas phase l, its momentum conservation equation is:

$$\begin{aligned}
&\frac{\partial}{\partial t}\left(\alpha_l \rho_l \overrightarrow{v}_l\right) + \nabla \cdot \left(\alpha_l \rho_l \overrightarrow{v}_l \overrightarrow{v}_l\right) \\
&\quad = -\alpha_l \nabla p + \nabla \cdot \overline{\overline{\tau}}_l + \alpha_l \rho_l \overrightarrow{g} \\
&\qquad + \overrightarrow{R}_{sl} + \dot{m}_{sl} \overrightarrow{v}_{sl} - \dot{m}_{ls} \overrightarrow{v}_{ls} \\
&\qquad + \left(\overrightarrow{F}_l + \overrightarrow{F}_{lift,l} + \overrightarrow{F}_{wl,l} + \overrightarrow{F}_{vm,l} + \overrightarrow{F}_{td,l}\right).
\end{aligned} \tag{5}$$

For the solid phase s,

$$\begin{aligned}
&\frac{\partial}{\partial t}\left(\alpha_s \rho_s \overrightarrow{v}_s\right) + \nabla \cdot \left(\alpha_s \rho_s \overrightarrow{v}_s \overrightarrow{v}_s\right) \\
&\quad = -\alpha_s \nabla p - \nabla p_s + \nabla \cdot \overline{\overline{\tau}}_s + \alpha_s \rho_s \overrightarrow{g} \\
&\qquad + \sum_{l=1}^{N}\left(\overrightarrow{R}_{ls} + \dot{m}_{ls} \overrightarrow{v}_{ls} - \dot{m}_{sl} \overrightarrow{v}_{sl}\right) \\
&\qquad + \left(\overrightarrow{F}_s + \overrightarrow{F}_{lift,s} + \overrightarrow{F}_{wl,s} + \overrightarrow{F}_{vm,s} + \overrightarrow{F}_{td,s}\right).
\end{aligned} \tag{6}$$

where $\overrightarrow{F}_l$ and $\overrightarrow{F}_s$ denote external body forces. $\overrightarrow{F}_{\text{lift},l}$ and $\overrightarrow{F}_{\text{lift},s}$ denote lift forces [26]. $\overrightarrow{F}_{wl,l}$ and $\overrightarrow{F}_{wl,s}$ denote wall lubrication forces (equal to zero as the no-sliding wall is used in this article). $\overrightarrow{F}_{vm,l}$ and $\overrightarrow{F}_{vm,s}$ are virtual mass forces [26]. $\overrightarrow{F}_{td,l}$ and $\overrightarrow{F}_{td,s}$ are turbulent dispersion forces. These forces have little effect on the examples presented in this article and are not considered for the sake of simplification. The remaining unknowns will be described as follows.

2.2.4. Other Equations. $\overrightarrow{R}_{sl}$ is the interaction force between the solid phase and the gas phase, which is defined as follows in ANSYS Fluent:

$$\overrightarrow{R}_{sl} = K_{sl}\left(\overrightarrow{v}_s - \overrightarrow{v}_l\right), \tag{7}$$

where $K_{sl}\,(= K_{ls})$ is the momentum exchange coefficient between phases. Gidaspow model [27] is used to describe K_{sl} in this article, which is a combination of the Wen and Yu model [28] and the Ergun equation [29]; the equations are as follows:

$$K_{sl} = \begin{cases} \dfrac{3}{4} C_D \dfrac{\alpha_s \alpha_l \rho_l \left|\overrightarrow{v}_s - \overrightarrow{v}_l\right|}{d_s} \alpha_l^{-2.65} & \alpha_l > 0.8, \\ 150 \dfrac{\alpha_s (1-\alpha_l)\mu_l}{\alpha_l d_s^2} + 1.75 \dfrac{\rho_l \alpha_s \left|\overrightarrow{v}_s - \overrightarrow{v}_l\right|}{d_s} & \alpha_l \le 0.8, \end{cases} \tag{8}$$

where

$$C_D = \frac{24}{\alpha_l \mathrm{Re}_s}\left[1 + 0.15\left(\alpha_l \mathrm{Re}_s\right)^{0.687}\right]. \tag{9}$$

$\overrightarrow{v}_{sl}$ is the interphase velocity expressed as follows:

$$\overrightarrow{v}_{sl} = \begin{cases} \overrightarrow{v}_s \text{ if} & \dot{m}_{sl} > 0, \\ \overrightarrow{v}_l \text{ if} & \dot{m}_{sl} < 0, \end{cases} \tag{10}$$

where $\dot{m}_{sl} > 0$ denotes the mass of solid phase and$s$ is transferred to the gas phase l; $\dot{m}_{sl} < 0$ denotes the mass of gas phase and l is transferred to the solid phase s. The definition of $\overrightarrow{v}_{ls}$ could be obtained in the same way. There is no mass transfer between the gas phase and the solid phase in this article so these terms could be set to 0.

p_s denotes the solid pressure of the solid phase s, which can be expressed as follows:

$$p_s = \alpha_s \rho_s \Theta_s + 2\rho_s\left(1 + e_{ss}\right)\alpha_s^2 g_{0,ss} \Theta_s, \tag{11}$$

where e_{ss} is the coefficient of restitution for particle collisions (0.9 by default), $g_{0,ss}$ is the radial distribution function [30, 31], and Θ_s denotes the granular temperature [32].

$\overline{\overline{\tau}}_l$ is the stress-strain tensor of the gas phase l, which can be expressed as follows:

$$\overline{\overline{\tau}}_l = \alpha_l \mu_l\left(\nabla \overrightarrow{v}_l + \nabla \overrightarrow{v}_l^{\,T}\right) + \alpha_l\left(\lambda_l - \frac{2}{3}\mu_l\right)\nabla \cdot \overrightarrow{v}_l \overline{\overline{I}}, \tag{12}$$

where μ_l and λ_l are shear viscosity and bulk viscosity of gas phase l, respectively.

$\overline{\overline{\tau}}_s$ is the stress-strain tensor of the solid phase s, which can be expressed as follows:

$$\overline{\overline{\tau}}_s = \alpha_s \mu_s\left(\nabla \overrightarrow{v}_s + \nabla \overrightarrow{v}_s^{\,T}\right) + \alpha_s\left(\lambda_s - \frac{2}{3}\mu_s\right)\nabla \cdot \overrightarrow{v}_s \overline{\overline{I}}, \tag{13}$$

where μ_s and λ_s are shear viscosity and bulk viscosity of solid phase s, respectively.

μ_s consists of the collisional viscosity, kinetic viscosity, and frictional viscosity in this article, which can be expressed as follows:

$$\mu_s = \mu_{s,\text{col}} + \mu_{s,\text{kin}} + \mu_{s,fr}, \tag{14}$$

where both collisional viscosity $\mu_{s,\text{col}}$ and kinetic viscosity $\mu_{s,\text{kin}}$ are described by the Gidaspow model and their expressions are as follows:

$$\mu_{s,\mathrm{kin}} = \frac{10\rho_s d_s\sqrt{\Theta_s\pi}}{96\alpha_s(1+e_{ss})g_{0,ss}}\left[1+\frac{4}{5}g_{0,ss}\alpha_s(1+e_{ss})\right]^2,$$
$$\mu_{s,\mathrm{col}} = \frac{4}{5}\alpha_s\rho_s d_s g_{0,ss}(1+e_{ss})\left(\frac{\Theta_s}{\pi}\right)^{1/2}. \tag{15}$$

The frictional viscosity $\mu_{s,fr}$ is described by the Schaeffer model [33], and its expression is as follows:

$$\mu_{s,fr} = \frac{p_{\mathrm{friction}}\sin\varphi}{2\sqrt{I_{2D}}}, \tag{16}$$

where p_{friction} denotes frictional pressure, φ is the internal friction angle, and I_{2D} is the second invariant of the deviatoric stress tensor.

The bulk viscosity of granular particles is described by the Lun et al. model [30], which can be expressed as follows:

$$\lambda_s = \frac{4}{3}\alpha_s^2\rho_s d_s g_{0,ss}(1+e_{ss})\left(\frac{\Theta_s}{\pi}\right)^{1/2}. \tag{17}$$

2.3. Turbulence Model. This section describes the influence of turbulent fluctuations on single-phase velocity and scalar; the shear stress transport (SST) $k-\omega$ model [34], a popular turbulence model in the field of engineering application at present with higher accuracy and credibility, was selected in this article. The SST $k-\omega$ model combines the advantages of the $k-\omega$ model in the near-wall region and the $k-\varepsilon$ model in the far-field and adds the transverse dissipation derivative term. In the definition of turbulent viscosity, the transport process of turbulent shear stress is considered, which is more widely applicable. In ANSYS Fluent, there are three kinds of multiphase flow turbulence models to choose from the SST $k-\omega$ model, which are mixed turbulence model, dispersed turbulence model, and per-phase turbulence model. The dispersion turbulence model is the appropriate choice when the second phase is dilute or the particle model is used; as a result, the dispersion turbulence model was selected for the simulation. The fluctuation amount of the second phase can be given according to the average characteristics of the main phase and the ratio of particle relaxation time to eddy current-particle interaction time in the dispersion turbulence model [35]. Therefore, only the gas phase is analyzed and calculated, and its transport equation is as follows:

$$\frac{\partial}{\partial t}(\rho_l k) + \nabla\cdot\left(\rho_l k\vec{U}_l\right) = \nabla\cdot(\Gamma_k\nabla k) + G_k - Y_k + S_k + G_b,$$
$$\frac{\partial}{\partial t}(\rho_l \omega) + \nabla\cdot\left(\rho_l \omega\vec{U}_l\right) = \nabla\cdot(\Gamma_\omega\nabla k) + G_\omega - Y_\omega + D_\omega + S_\omega + G_{\omega b}, \tag{18}$$

where $\vec{U}_l$ denotes the average velocity of the gas phase; G_k and G_ω denote the turbulence kinetic energy k and specific dissipation rate ω (the ratio of turbulence dissipation ε to turbulent kinetic energy k) generated by the velocity gradient separately. Γ_k and Γ_ω denote effective diffusivity of k and ω, respectively. Y_k and Y_ω are the dissipation of k and ω due to turbulence separately, and D_ω is the cross-diffusion term. S_k and S_ω are source terms; G_b and $G_{\omega b}$ denote the buoyancy terms. The source terms and buoyancy terms have little influence on our calculation, which are not considered here for the sake of simplification. The specific meaning of each item can refer to ANSYS Fluent's theory guide.

2.4. Fluent Parameter Settings. The gas phase is set to nitrogen in this article and the data in the Fluent material database can be used. The solid phase is set as ultrafine dry powder particles, and its physical parameters are set as shown in Table 1. The Gidaspow model is used to describe the drag coefficient between ultrafine dry powder and nitrogen. The collision recovery coefficient between particles is set as 0.9 [36].

The filling ratio of nitrogen and ultrafine dry powder is set as 15 L/kg in this article. According to the density of nitrogen and ultrafine dry powder set, the volume proportion of ultrafine dry powder at the pipeline inlet is about 3.8%. The setting of boundary conditions is shown in Table 2.

It should be noted that the static pressure values and full pressure values of the two inlets are all set to 1.5×10^5 Pa - 1.5×10^6 Pa to simulate the pure pressure-driven flow. It is found that when the pressure values of the two inlets are different, the ultrafine dry powder will flow out of the inlet_gas (the pressure value of blow-assisted nitrogen is less than that of ultrafine dry powder), or nitrogen will inhibit the release of dry powder (the pressure value of blow-assisted nitrogen is greater than that of ultrafine dry powder). Therefore, we set the pressure value of the two inlets to be the same to avoid this phenomenon.

3. Mesh Independency Study and Experimental Variation

A grid independence test was conducted in order to verify the relationship between the simulation results and the number of grids. The grid data are shown in Table 3, and the number of grid nodes has roughly doubled. The calculation results are changed slightly with the increase of the number of grids through calculation, as shown in Figure 5. To save calculation time, the grid file with the number of grid nodes as 79332 is accepted for simulation calculation under different working conditions.

Experiments were conducted to verify the simulations. After the pressure in the tank reaches a certain value, the valves are opened for 10 seconds and closed immediately. The pressure in the tank is assumed to be constant for this extremely short period of time, and the dry powder in the recovery unit and pipe is collected to evaluate the mass flow rate. The experimental results are much smaller than the results of simulation due to the long transportation, but the calculated values in Figure 6 show that the simulation results could have reference value in the optimization process according to the following equations.

Table 1: Properties of superfine dry powder particle.

Properties	Parameter settings
Density (kg/m3)	1760
Diameter (m)	1.87×10−5
Granular viscosity (kg/m·s)	Gidaspow
Granular bulk viscosity (kg/m·s)	Lun et al.
Solids pressure (Pa)	Lun et al.
Granular temperature (m2/s2)	Algebraic
Fraction viscosity (kg/m·s)	Schaeffer
Frictional pressure (Pa)	KTGF-based
Friction packing limit	0.61
Angel of internal friction (deg)	30
Packing limit	0.63
Radial distribution	Lun et al.

Table 2: Boundary conditions.

Boundary	Type	Settings
inlet_gas	Pressure inlet	1.5×10^5 Pa–1.0×10^6 Pa
inlet_mixture	Pressure inlet	1.5×10^5 Pa–1.0×106 Pa
Outlet	Pressure outlet	101325 Pa
Wall	Stationary wall	Roughness height 0.0002 m

Table 3: Mesh statistics of different element size.

Element size (m)	Nodes	Elements
0.0085	40864	102942
0.005	79332	222758
0.0035	160457	493939
0.0025	324119	1034691

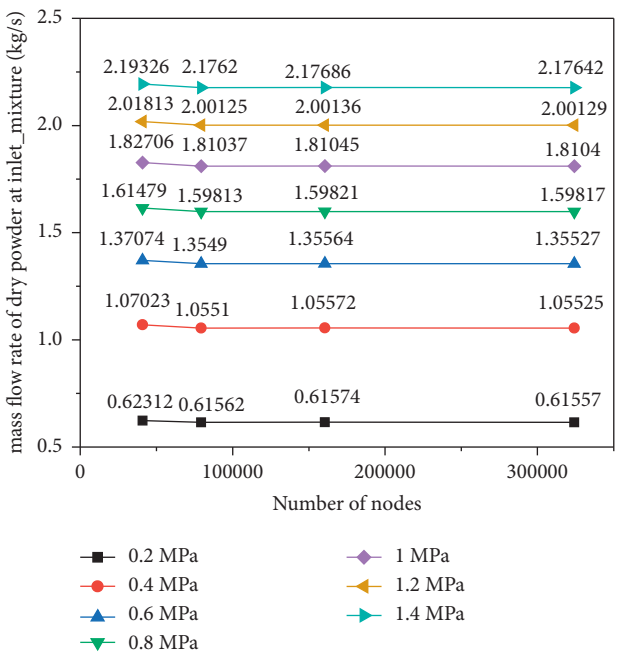

Figure 5: Comparison of calculation results under different inlet pressures and different mesh sizes.

$$Q = \sqrt{\Delta P/(\rho g s l)}, \tag{19}$$

where s and l denote the flow resistance and length of pipe, respectively. The length of the pipe in the experiment is 25.645 m and the length of the pipe in simulation is 1.284 m, which could be substituted into equation (19) to get that the experimental result should be about 0.2236 times the simulation result under the same pressure conditions. The experimental results are lower than the calculated values due to the several bends of the pipe and a small account of the escaped dry powder, which increase the flow resistance and decrease the mass of the collected dry powder, respectively.

4. Results and Analysis

The calculation results of the mass flow rate of ultrafine dry powder and nitrogen at inlets under different inlet pressures are shown in Figure 6. It can be found that the mass flow rates of ultrafine dry powder and nitrogen show a growth at the beginning part of the curve. As the inlet pressure continues to increase, the growth rate has gradually stabilized, showing a roughly linear growth. It could also be found from Figure 7 that the nitrogen mass flow rate at different inlets increases as the inlet pressure increases, and the difference of nitrogen mass flow rate at two inlets becomes more obvious. Moreover, the growth rates of the two curves of nitrogen mass flow rate are obviously different.

The calculation results of the velocities of the ultrafine dry powder and nitrogen at two inlets and outlet of the pipeline under different inlet pressures are shown in Figure 8. It could be seen from the figure that the velocity difference between the ultrafine dry powder and nitrogen is not obvious, and the velocity curves of the two are approximately coincident at the inlet_mixture as the inlet pressure increases. However, due to the addition of pressurized nitrogen, the velocity of nitrogen at the outlet increases obviously, and the velocity gap between nitrogen and ultrafine dry powder gradually widens as the inlet pressure increases. Therefore, it could be clearly observed in Figure 8 that there is a clear gap between the velocity curves of ultrafine dry powder and nitrogen at the outlet, and the nitrogen velocity difference at the two inlets also increases as the inlet pressure increases, which corresponds to the mass flow rate curves in Figure 7.

The mass flow rate of ultrafine dry powder determines the efficiency of fire extinguishing, and the flow velocity of ultrafine dry powder determines its transport height and spray distance. These two parameters are of great significance for fire suppression. The diameter of the nitrogen-assisted blowing pipe, the diameter of the outlet pipe, and the inlet diameter of the mixing pipe (as shown in Figure 9) will all affect the release of ultrafine dry powder. The following will focus on analyzing the changes of these three parameters on the mass flow rate and velocity of ultrafine dry powder.

4.1. The Influence of the Diameter of the Nitrogen-Assisted Blowing Pipe on the Flow Field in the Pipe. As shown in Figure 10, under the same inlet pressure, the mass flow

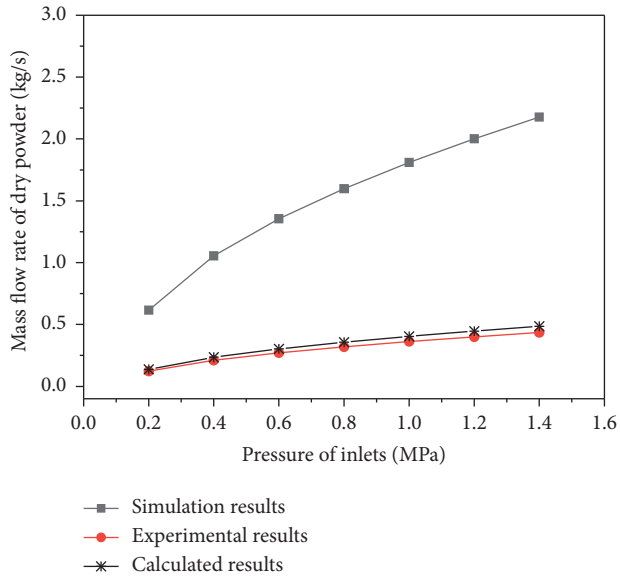

Figure 6: Comparison of the experimental results, simulation results and calculated results.

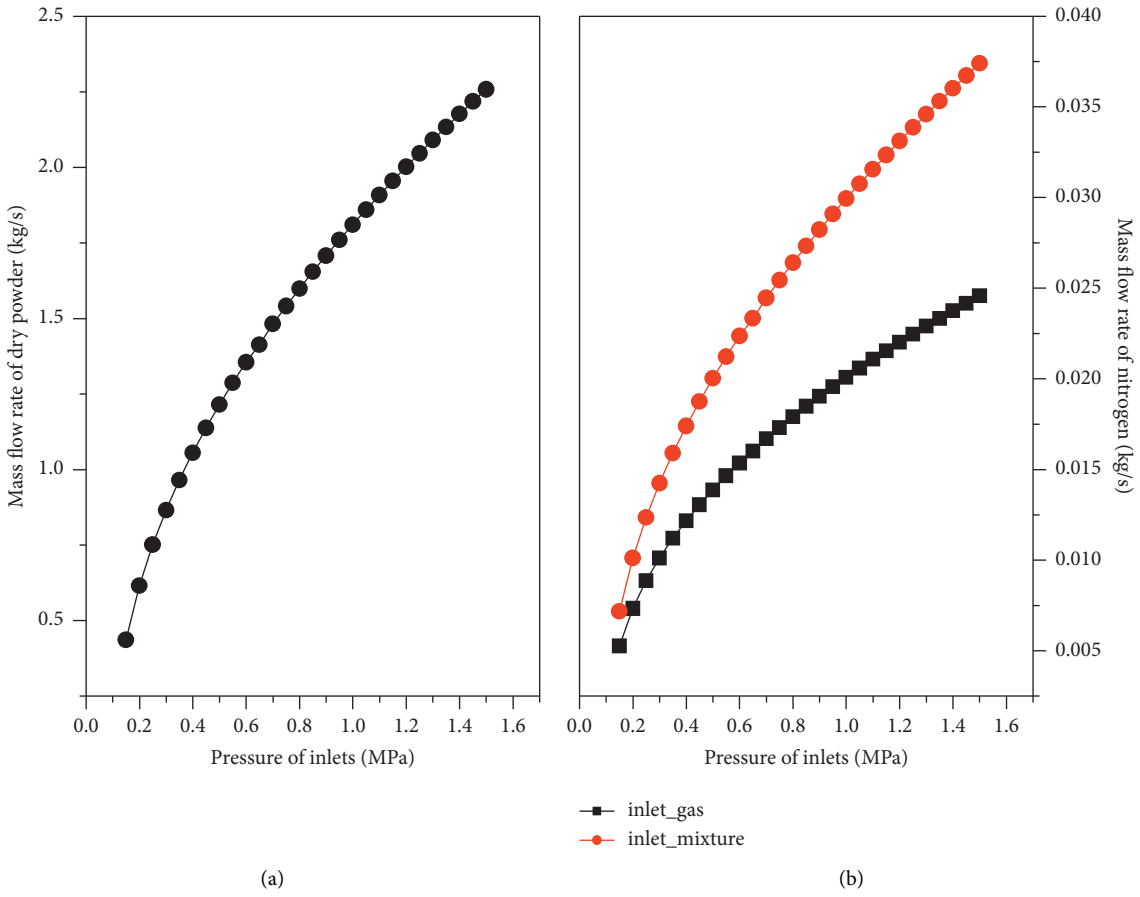

Figure 7: The mass flow curves of ultrafine dry powder and nitrogen at inlets under different inlet pressure.

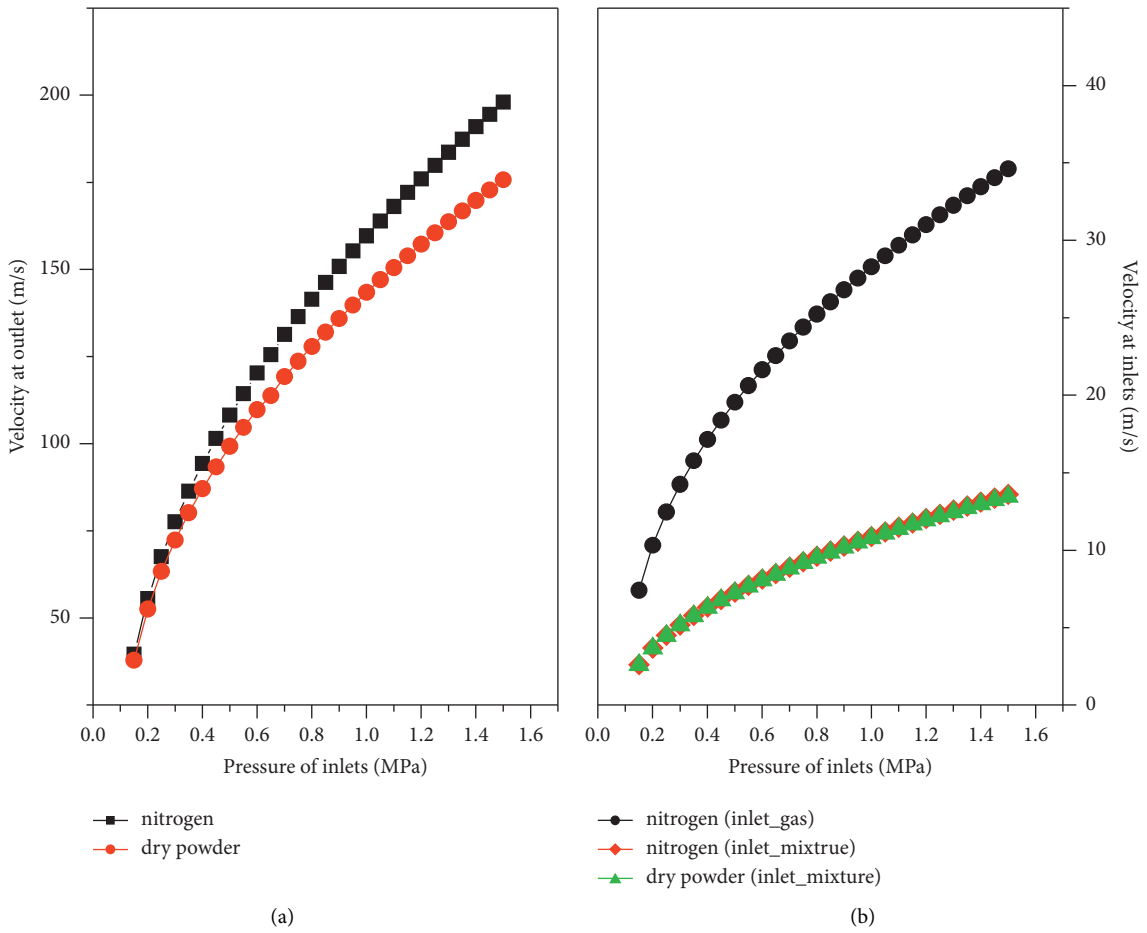

Figure 8: The velocity of ultrafine dry powder and nitrogen at inlet_mixture and outlet vary with inlet pressure.

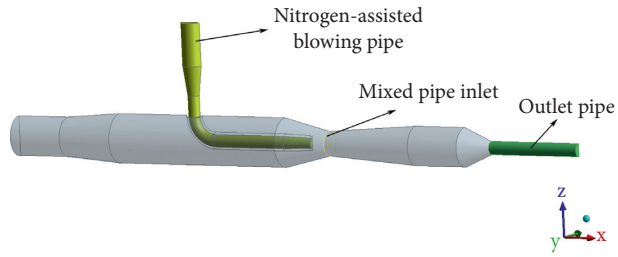

Figure 9: The position of nitrogen-assisted blowing pipe, outlet pipe and mixed pipe inlet.

rate of ultrafine dry powder will decrease when increasing the diameter of the nitrogen-assisted blowing pipe. The velocity of ultrafine dry powder at the outlet changes drastically, as shown in Figure 11. Obviously, under the same inlet pressure, the increase in the diameter of the nitrogen-assisted blowing pipe can greatly increase the velocity of the ultrafine dry powder at the outlet.

The velocity distribution contour diagram and volume fraction contour diagram at the pipe symmetry plane under the condition of 0.6 MPa inlet pressure are shown in Figures 12 and 13 separately. It could be found that increasing

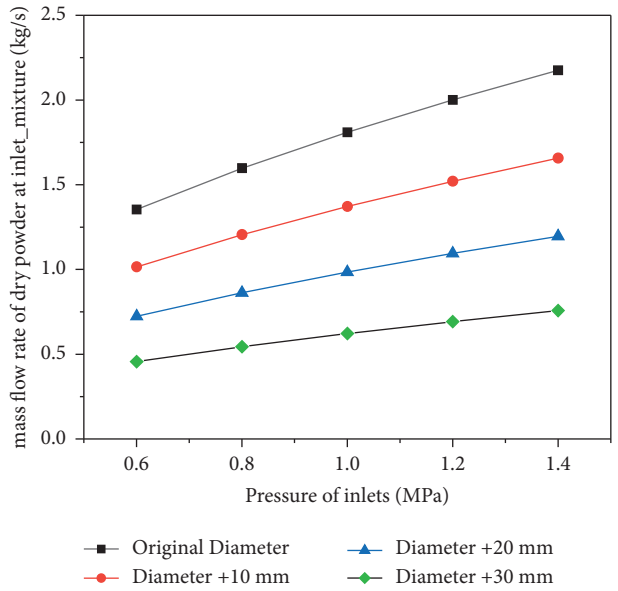

Figure 10: The mass flow rate of ultrafine dry powder at inlet_mixture varies with inlet pressure under different nitrogen-assisted blowing pipe diameter.

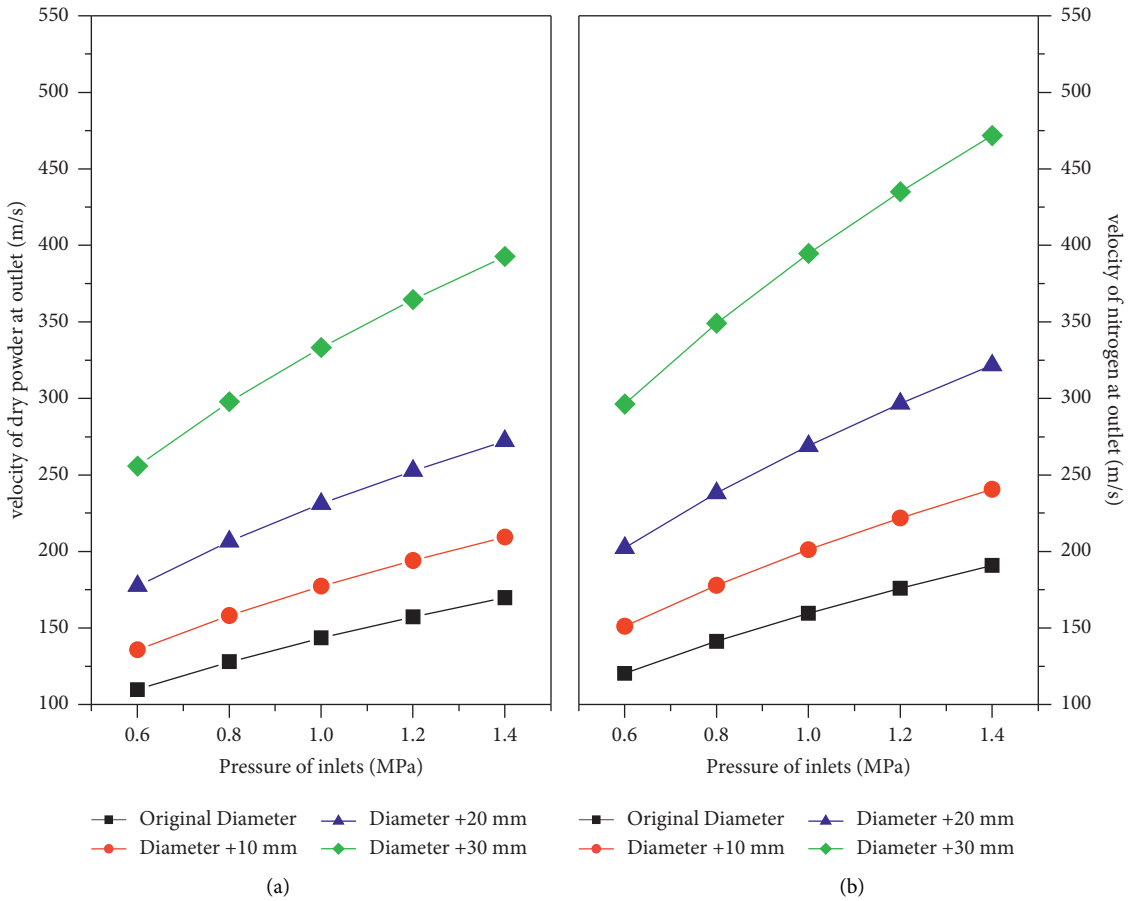

Figure 11: Ultrafine dry powder and nitrogen velocity at outlet varies with inlet pressure under different nitrogen-assisted blowing diameter.

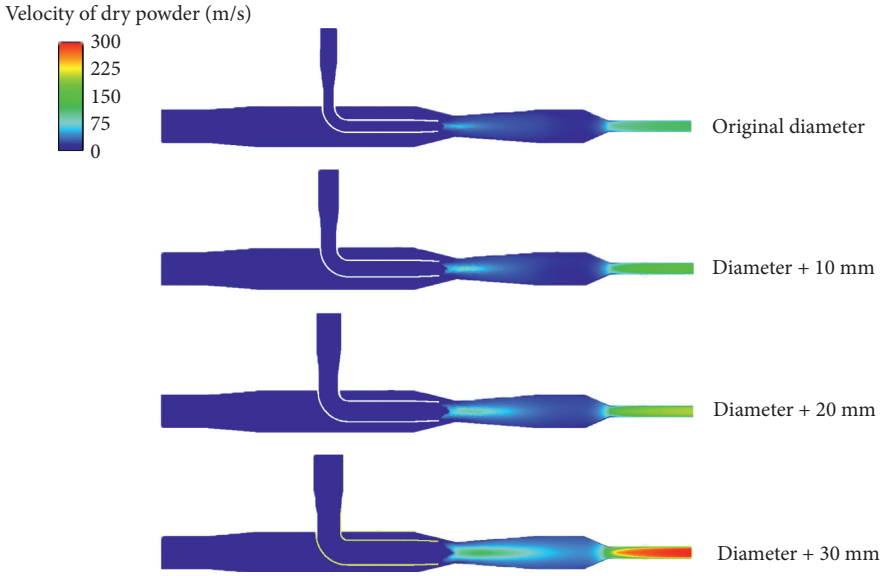

Figure 12: Contour diagram of velocity distribution at the symmetrical surface of pipe under different diameters of nitrogen-assisted blowing pipe (inlet pressure: 0.6 MPa).

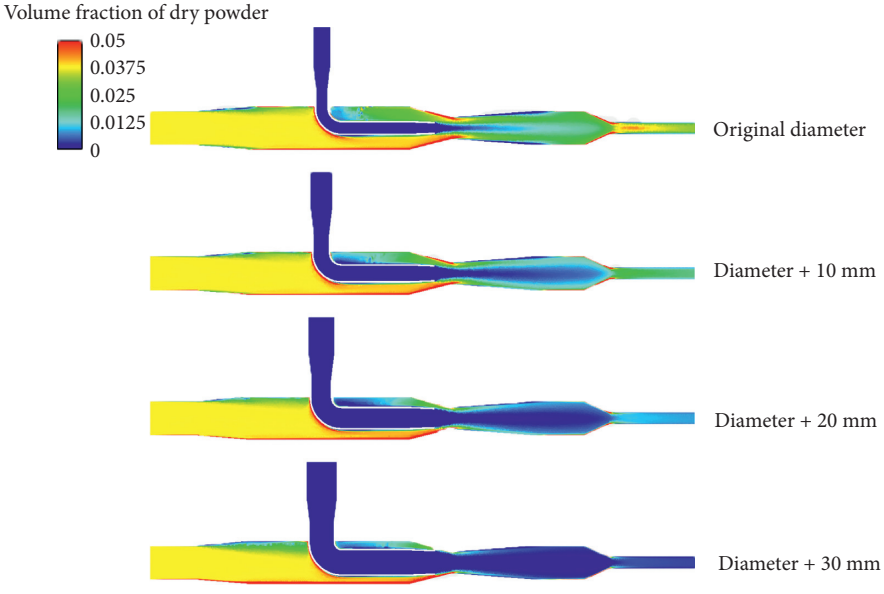

Figure 13: Contour diagram of the distribution of ultrafine dry powder volume fraction at the symmetrical surface of the pipe under different diameters of nitrogen-assisted blowing pipe (inlet pressure: 0.6 MPa).

the diameter of the nitrogen-assisted blowing pipe can increase the flow velocity of the ultrafine dry powder at the outlet, but it hinders the flow of the ultrafine dry powder in the pipe, causing the ultrafine dry powder to easily stay in the front part of the pipe. This situation may be improved if the diameter of the inlet of the mixing pipe is increased, which will be discussed as follows.

4.2. The Influence of the Outlet Pipe Diameter on the Flow Field in the Pipe. The influence of the variation of outlet pipe diameter on the mass flow rate of ultrafine dry powder is shown in Figure 14. It could be seen from the figure that under the same inlet pressure, increasing the diameter of the outlet pipe will increase the mass flow rate of ultrafine dry powder. The influence of changing the outlet pipe diameter

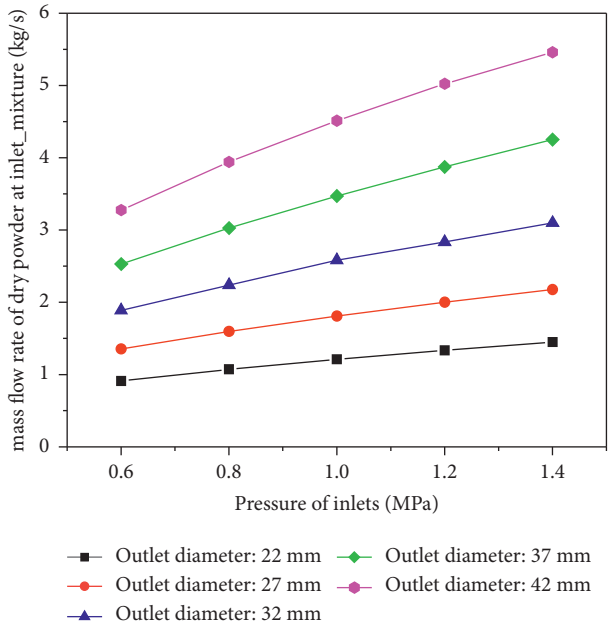

Figure 14: Variation of ultrafine dry powder mass flow rate at inlet_mixture with inlet pressure under different outlet pipe diameters.

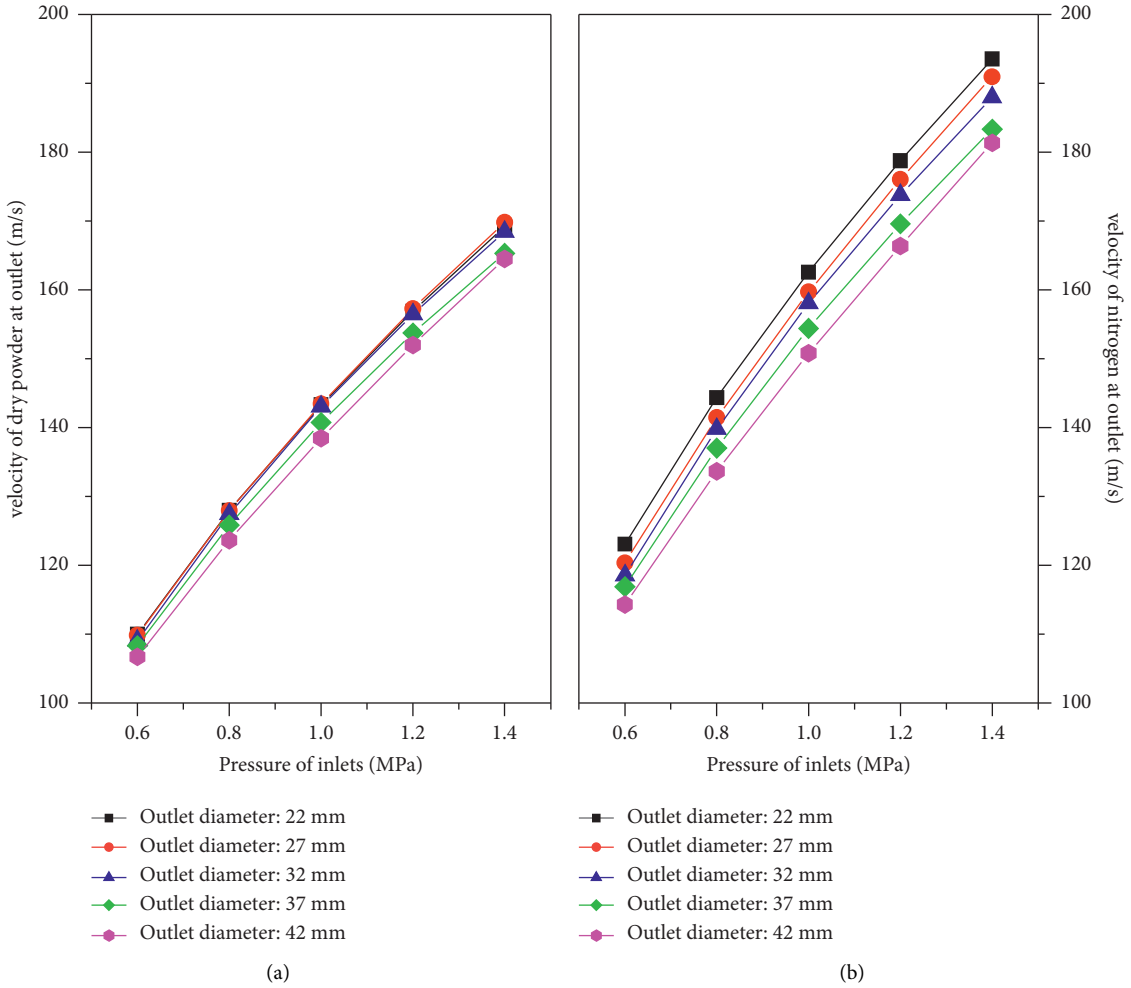

Figure 15: Ultrafine dry powder and nitrogen velocity at outlet vary with inlet pressure under different diameters of outlet pipe.

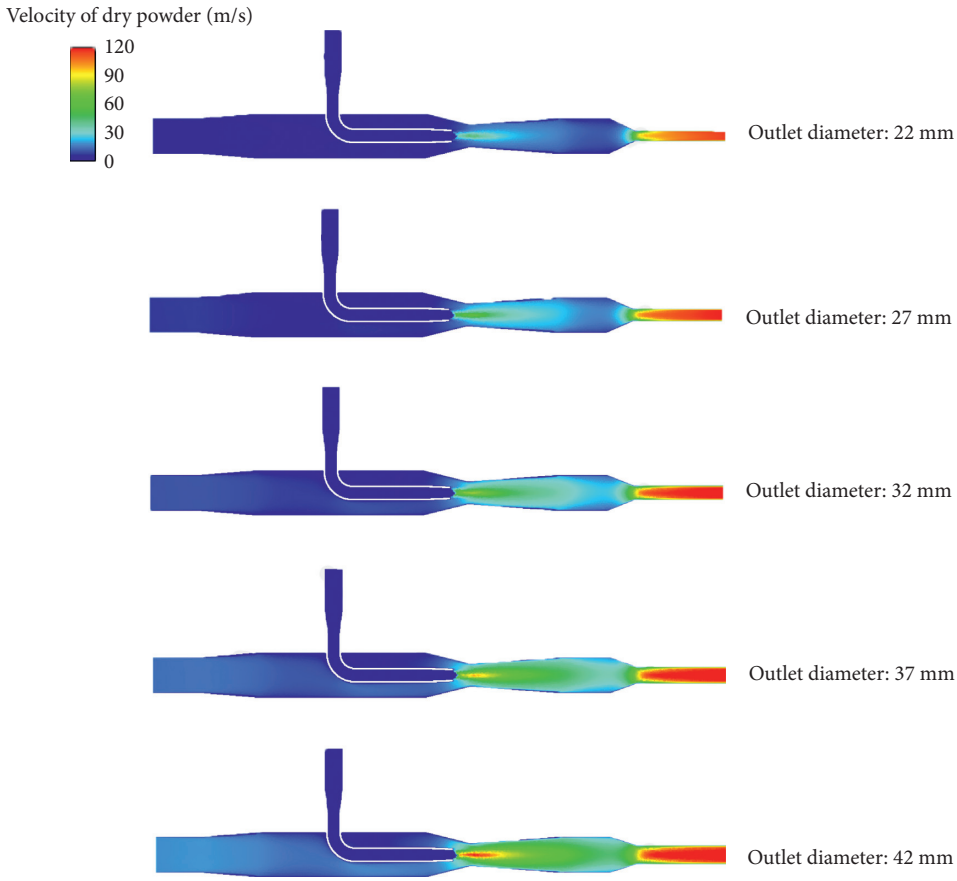

Figure 16: Contour diagram of velocity distribution at the symmetrical surface of pipe under different diameters of outlet pipe (inlet pressure: 0.6 MPa).

on the velocity of ultrafine dry powder at the outlet is shown in Figure 15. It could be seen from the figure that increasing the diameter of the outlet pipe has a relatively small effect on the velocity of the ultrafine dry powder at the outlet. Only when the diameter of the outlet pipe is increased to a certain extent, the obvious velocity drop will appear.

The velocity distribution contour diagram and volume fraction contour diagram at the pipe symmetry plane under the condition of 0.6 MPa inlet pressure are shown in Figures 16 and 17. It could be seen from the figures that the increasing the diameter of the outlet pipe makes the distribution of the ultrafine dry powder in the outlet pipe more uniform, and the velocity in the mixing pipe is obviously improved, and the velocity in the remaining areas has also been improved to a certain extent. The increase in the velocity of ultrafine dry powder in the pipeline causes a certain range of area (blue area) with lower ultrafine dry powder content around the elbow of the nitrogen-assisted blowing pipe, and this area increases with the increase in the diameter of the outlet pipe.

4.3. Influence of Inlet Diameter of Mixing Pipe on the Flow Field in the Pipe. The influence of changing the inlet diameter of the mixing pipe on the mass flow rate of ultrafine dry powder is shown in Figure 18. It could be seen from the figure that under the same inlet pressure, increasing the inlet diameter of the mixing pipe will increase the mass flow rate of ultrafine dry powder entering the pipe, and the effect will be weakened with the increase of the inlet diameter of the mixing pipe. It could be seen that the influence of the inlet diameter of the mixing pipe on the mass flow rate of ultrafine dry powder entering the pipe is not a simple linear relationship, and the increase of its diameter will promote the release of ultrafine dry powder. The influence of changing the inlet diameter of the mixing pipe on the velocity of dry powder and at the outlet of the pipe is shown in Figure 19. As can be seen from the figure, under the same inlet pressure, increasing the inlet diameter of the mixing pipe would decrease the flow velocity of dry powder at the pipe outlet.

The velocity distribution contour diagram and volume fraction contour diagram at the pipe symmetry plane under the condition of 0.6 MPa inlet pressure are shown in

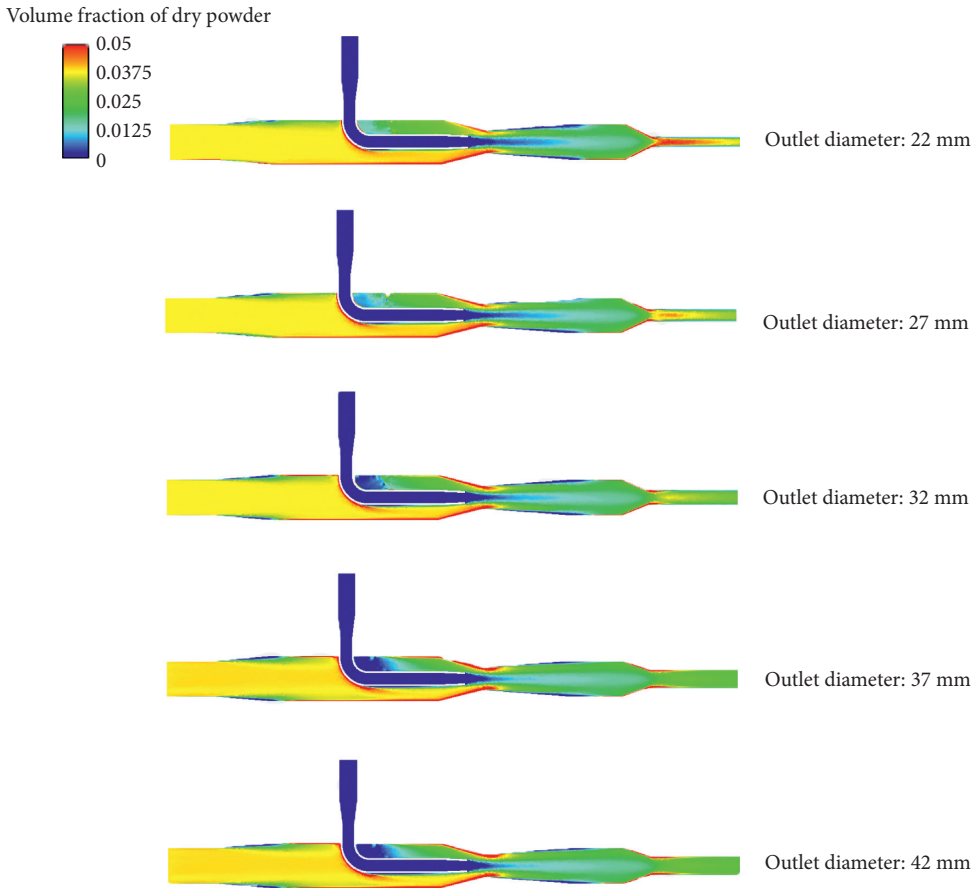

Figure 17: Contour diagram of the distribution of ultrafine dry powder volume fraction at the symmetrical surface of the pipe under different diameters of outlet pipe (inlet pressure: 0.6 MPa).

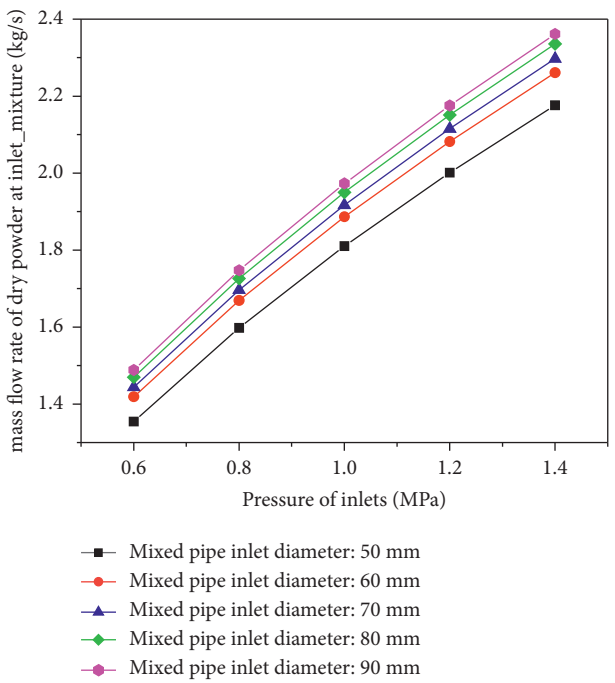

Figure 18: Variation of dry powder mass flow rate at inlet_mixture with inlet pressure under different diameters of mixed pipe inlet.

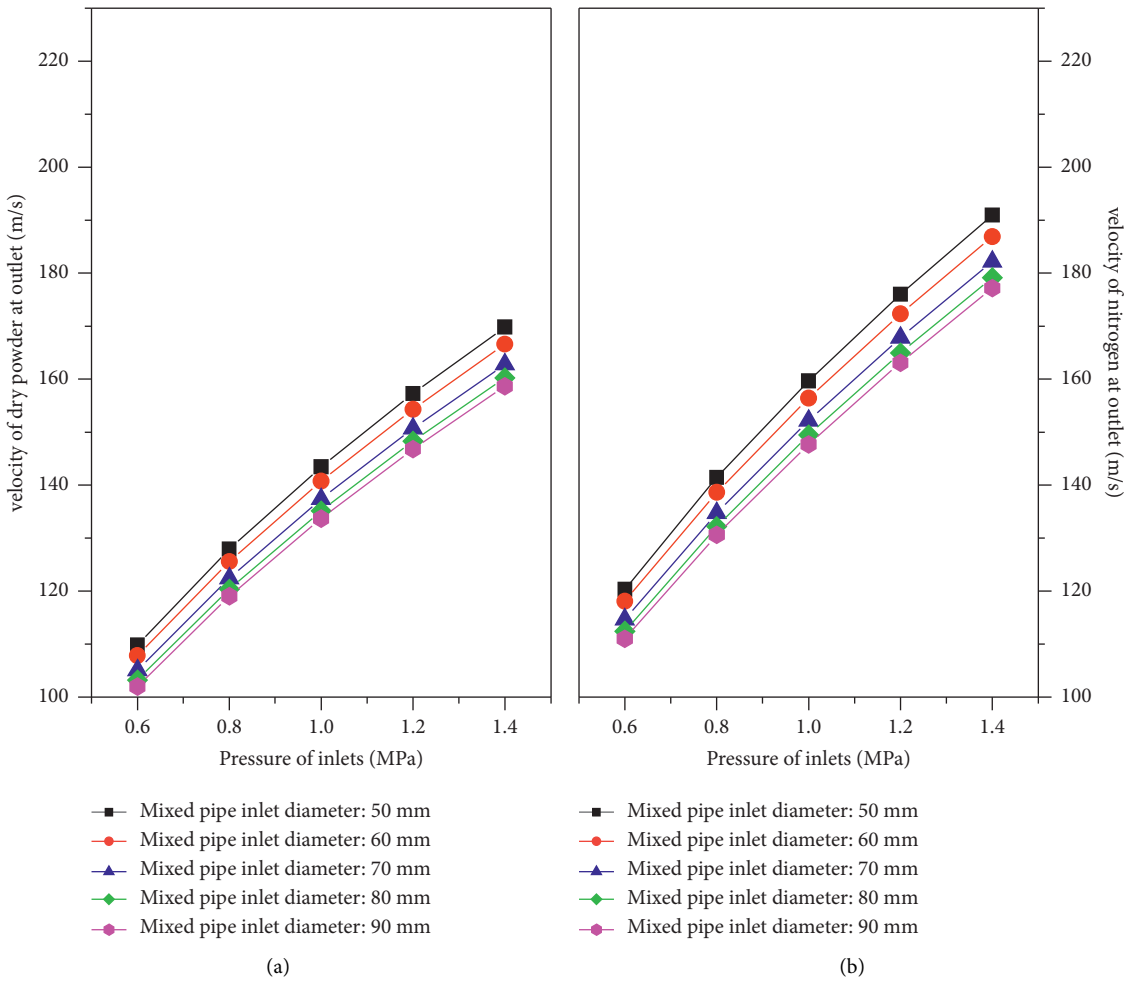

Figure 19: Ultrafine dry powder and nitrogen velocity at outlet varies with inlet pressure under different diameters of mixed pipe inlet.

Figures 20 and 21. As can be seen from the figures, the increase of the inlet diameter of the mixing pipe decreases the velocity of the ultrafine dry powder in the mixing pipe but increases the volume fraction of the ultrafine dry powder in the outlet pipe, so the mass flow rate of the ultrafine dry powder increases when the outlet velocity decreases.

In conclusion, increasing the inlet diameter of the mixing pipe is beneficial to the blow-assisted effect of ultrafine dry powder. Although it decreases the flow velocity of ultrafine dry powder in the outlet pipe to a certain extent, it also decreases the obstruction of ultrafine dry powder flow in the pipeline so that the mass flow rate of ultrafine dry powder is improved. The flow velocity of ultrafine dry powder in the outlet pipe could be compensated by changing size parameters of other positions, such as appropriately increasing the diameter of the nitrogen-assisted blowing pipe to increase the velocity of nitrogen or appropriately adjusting the diameter of the outlet pipe to accelerate the flow velocity of ultrafine dry powder.

4.4. Comparison of Several Improvement Schemes. According to the above analysis, six improved size schemes are determined, and the specific size parameters are shown in Table 4. The comparison between the improved schemes and the original scheme is shown in Figure 22. As can be seen from Figure 22, compared with the original scheme, the ultrafine dry powder outlet velocity of these schemes is higher than that of the original scheme under the same inlet pressure. However, only two schemes, P2 and P4, have higher ultrafine dry powder mass flow rates than the original scheme. Thus, it could be concluded that when the diameter increase of the nitrogen-assisted blowing pipe is between 10 mm and 20 mm, the diameter of the outlet pipe is 32 mm,

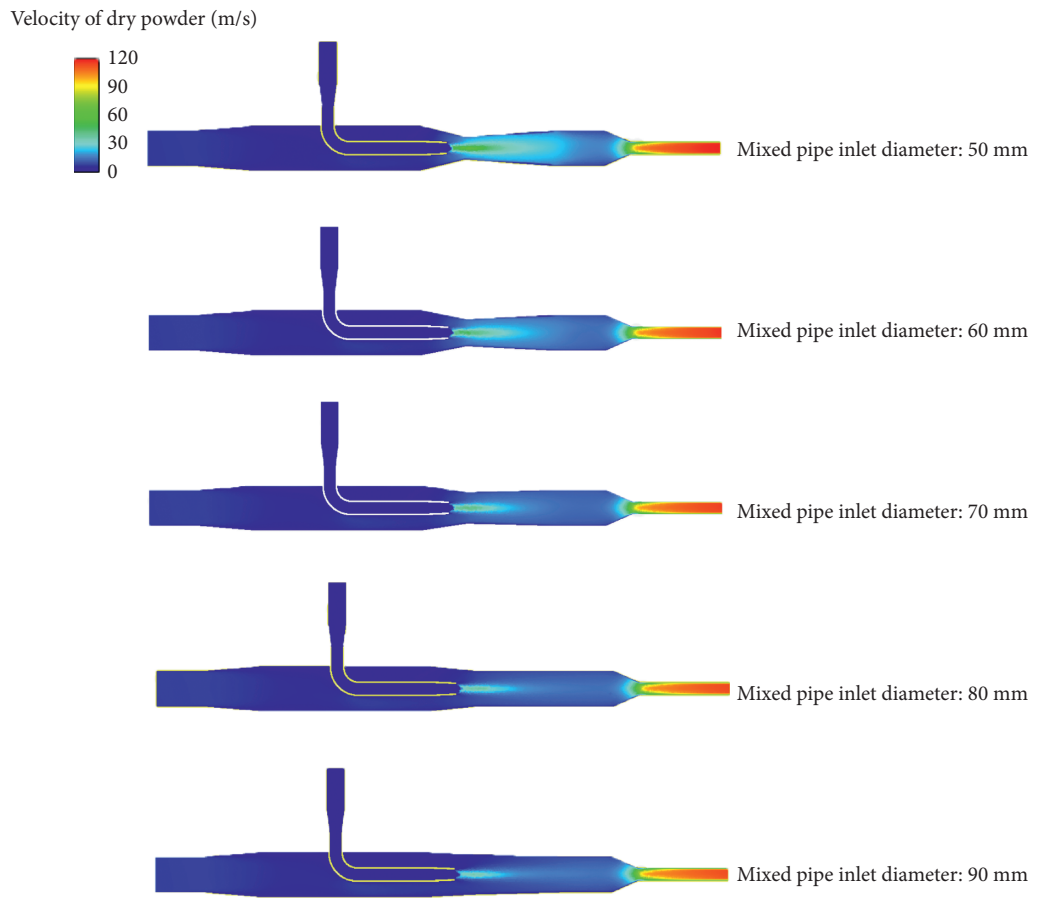

Figure 20: Contour diagram of velocity distribution at the symmetrical surface of pipeline under different diameters of mixed pipe inlet (inlet pressure: 0.6 MPa).

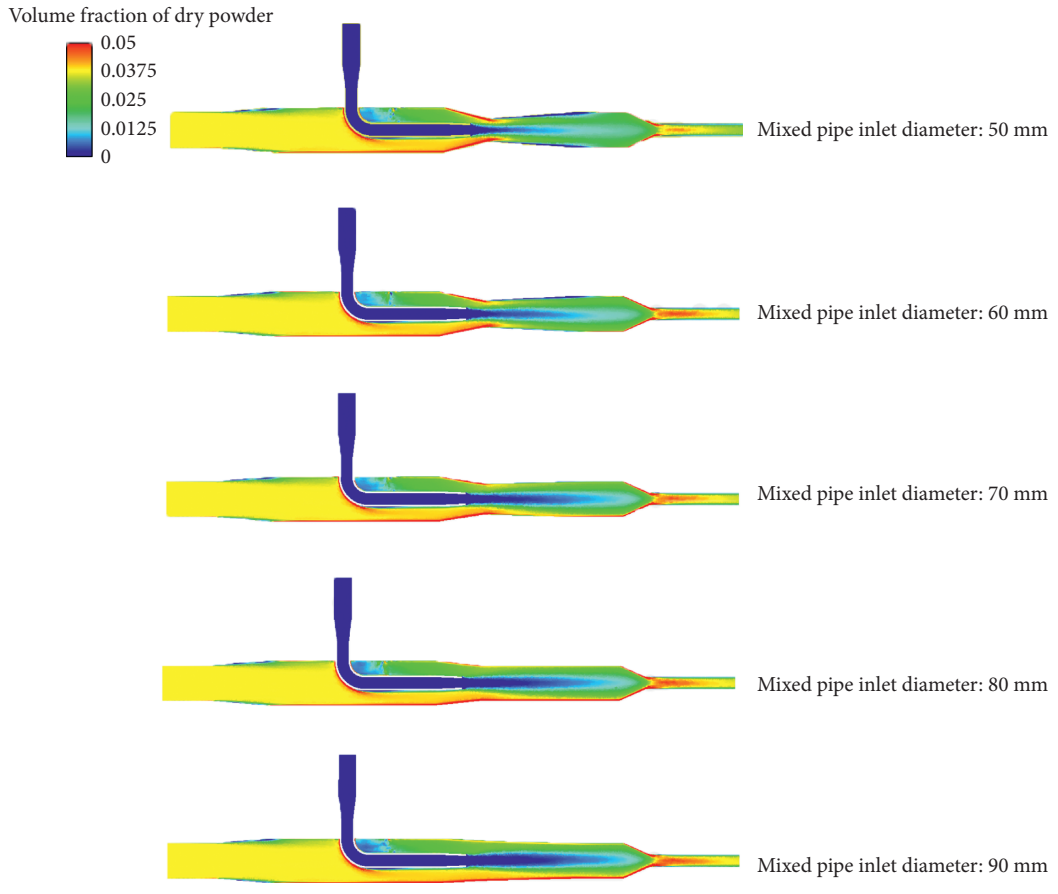

Figure 21: Contour diagram of the distribution of ultrafine dry powder volume fraction at the symmetrical surface of the pipe under different diameters of mixed pipe inlet (inlet pressure: 0.6 MPa).

Table 4: Size parameters of different improved schemes.

Scheme code	Diameter of the nitrogen-assisted blowing pipe (mm)	Diameter of outlet pipe (mm)	Inlet diameter of mixing pipe (mm)
P1	+10	27	90
P2	+10	32	90
P3	+20	27	90
P4	+20	32	90
P5	+30	27	90
P6	+30	32	90

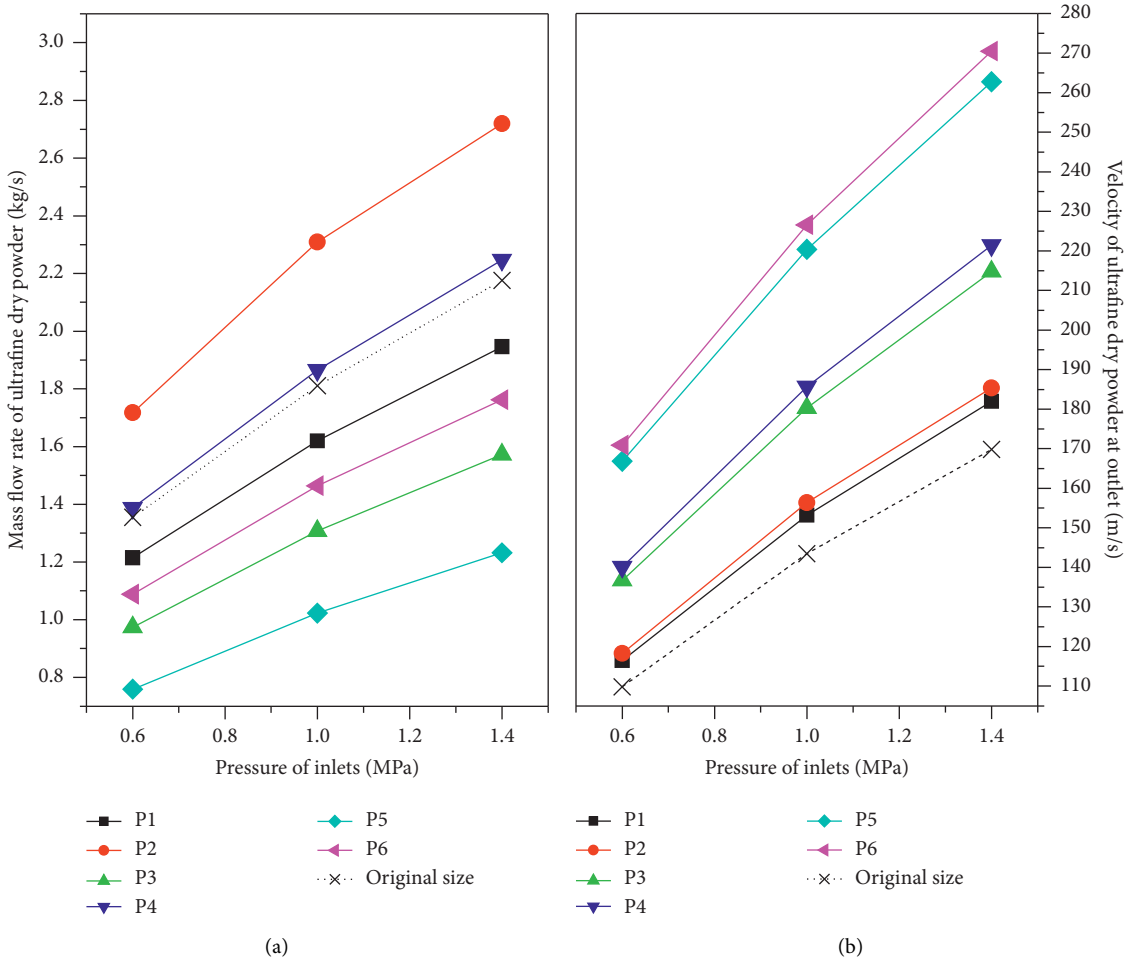

Figure 22: The ultrafine dry powder mass flow rate and outlet velocity of six improved schemes were compared with the original size scheme.

and the diameter of the mixing pipe inlet is 90 mm, and the mass flow rate of the ultrafine dry powder and the velocity at the outlet could be improved compared with the original pipe.

5. Conclusions

In this article, the influence of different inlet pressures on the mass flow rate and velocity of ultrafine dry powder and nitrogen in the existing blow-assisted pipe is determined by calculating and analyzing the internal flow field of the pipe at first, and the range of approximate linear variation of the curve is determined, which saves time for the following calculation. Then we changed the size parameters of three parts of the blow-assisted pipe: the diameter of the nitrogen-assisted blowing pipe, the diameter of the outlet pipe, and the inlet diameter of the mixing pipe. These parameters are analyzed to the effect of mass flow rate and velocity of the ultrafine dry powder and nitrogen in the pipe within the range of inlet pressures. Under the same inlet pressure, the conclusions obtained are as follows:

(1) Increasing the diameter of the nitrogen-assisted blowing pipe on the existing blow-assisted pipe can increase the flow velocity of the ultrafine dry powder in the outlet pipe. However, the increase of the diameter of the nitrogen-assisted blowing pipe will

hinder the passage of the ultrafine dry powder, resulting in the decrease of the mass flow rate of the ultrafine dry powder.

(2) Increasing the diameter of the outlet pipe will increase the mass flow rate and velocity of ultrafine dry powder entering the pipe and decrease the mass flow rate of ultrafine dry powder in the outlet pipe, while the decreasing effect of the ultrafine dry powder velocity is relatively weak. Better nitrogen blowing effect could be achieved by increasing the diameter of the outlet pipe slightly.

(3) blowing The increase of the inlet diameter of the mixing pipe will increase the mass flow rate and velocity of the ultrafine dry powder from the dry powder tank into the pipe and slightly decrease the flow velocity of ultrafine dry powder at the outlet of the pipe. It is beneficial to promote the release of the dry powder and adjust other size parameters could help to achieve the best effect of nitrogen-assisted .

(4) Through the calculation and analysis of the six improvement schemes, it could be obtained that when the diameter of the nitrogen-assisted blowing pipe is increased between 10 mm and 20 mm, the diameter of the outlet pipe is 32 mm, and the diameter of the inlet of the mixing pipe is 90 mm, compared with the original pipe, the mass flow rate of ultrafine dry powder and the velocity at the outlet can be improved.

Nomenclature

q: The phase of fluid/solid
V: The volume of the phase
$\dot{m}_{pq}$: Mass transfer from phase p to q per second
$\dot{m}_{qp}$: Mass transfer from phase q to p per second
$\vec{v}$: The velocity of the phase (m/s)
$\vec{F}_l$, $\vec{F}_s$: External body forces (N)
$\vec{F}_{lift,l}$, $\vec{F}_{lift,s}$: Lift forces (N)
$\vec{F}_{wl,l}$, $\vec{F}_{wl,s}$: Wall lubrication forces (N)
$\vec{F}_{vm,l}$, $\vec{F}_{vm,s}$: Virtual mass forces (N)
$\vec{F}_{t\ d,l}$, $\vec{F}_{t\ d,s}$: Turbulent dispersion forces (N)
R_{sl}: The interaction force between the solid phase and the gas phase (N)
K_{sl}, K_{ls}: The momentum exchange coefficient between phases
Re: Reynolds number
d_s: Diameter of the particles
p_s: The solid pressure of the solid phase
e_{ss}: The coefficient of restitution for particle collisions
$g_{0,ss}$: The radial distribution function
p_{friction}: The frictional pressure (Pa)
I_{2D}: The second invariant of the deviatoric stress tensor
$\vec{U}_l$: The average velocity of the gas
G_k and G_ω: Turbulence kinetic energy k and specific dissipation rate ω
k: Turbulence kinetic energy
Y_k and Y_ω: The dissipation of k and ω due to turbulence
D_ω: The cross-diffusion term
S_k and S_ω: The source terms
G_b and G_{wb}: The buoyancy terms

Greek

α: The volume fraction of the phase
ρ: Density (kg/m³)
$\hat{\rho}$: Effective density (kg/m³)
$\underline{\rho}_{rq}$: The phase reference density (kg/m³)
$\overline{\overline{\tau}}$: The stress-strain tensor of the phase
Θ_s: Granular temperature (K)
μ and λ: Shear viscosity and bulk viscosity (Pa·s)
$\mu_{s,col}$: The collisional viscosity (Pa·s)
$\mu_{s,kin}$: The kinetic viscosity (Pa·s)
$\mu_{s,fr}$: The frictional viscosity (Pa·s)
φ: The internal friction angle (°)
ω: The specific dissipation rate (the ratio of turbulence dissipation ε to turbulent kinetic energy k)
Γ_k and Γ_ω: The effective diffusivity of k and ω

Subscripts

CFD: Computational fluid dynamics.

Data Availability

The datasets generated and/or analyzed during the current study are not publicly available due to the geometry and mesh files of our study containing confidential information but are available from the corresponding author on reasonable request.

Conflicts of Interest

The authors declare that they have no conflicts of interest.

Authors' Contributions

Bin Miao and Fanbao Chen contributed to the conceptualization and validation; Fanbao Chen contributed to methodology, provided the software, reviewed and edited the article, performed visualization, performed supervision, performed project administration, and was responsible for funding acquisition; Bin Miao was performed formal analysis, performed investigation, provided resources, performed data curation, and wrote the original draft. All authors have read and agreed to the published version of the manuscript.

Acknowledgments

This study was funded by the School of Safety Engineering and School of Resources and Geosciences in China University of Mining and Technology.

References

[1] X. Liu, H. Zhang, and Q. Zhu, "Factor analysis of high-rise building fires reasons and fire protection measures," *Procedia Engineering*, vol. 45, pp. 643–648, 2012.

[2] R. G. Hynes, J. C. Mackie, and A. R. Masri, "Shock-tube study of the pyrolysis of the halon replacement molecule CF3CHFCF3," *The Journal of Physical Chemistry A*, vol. 103, no. 1, pp. 54–61, 1999.

[3] T. K. Al-Awad, M. N. Saidan, and B. J. Gareau, "Halon management and ozone-depleting substances control in Jordan," *International Environmental Agreements: Politics, Law and Economics*, vol. 18, no. 3, pp. 391–408, 2018.

[4] M. J. Molina and F. S. Rowland, "CFCs in the environment," *Nature*, vol. 8, 1974.

[5] N. Saito, Y. Saso, Y. Ogawa, Y. Otsu, and H. Kikui, "Fire extinguishing effect of mixed agents of Halon 1301 and inert gases," *Fire Safety Science*, vol. 5, pp. 901–910, 1997.

[6] P. Laffitte, R. Delbourgo, J. Combourieu, and J. C. Dumont, "The influence of particle diameter on the specificity of fine powders in the extinction of flames," *Combustion and Flame*, vol. 9, no. 4, pp. 357–367, 1965.

[7] G. C. Harrison, *Solid Particle Fire Extineuishants for Aircraft Auulications*, Walter Kidde Aerospace, Wilson, North Carolina, 1993.

[8] C. T. Ewing, F. R. Faith, J. B. Romans, J. T. Hughes, and H. W. Carhart, "Flame extinguishment properties of dry chemicals: extinction weights for small diffusion pan fires and additional evidence for flame extinguishment by thermal mechanisms," *Journal of Fire Protection Engineering*, vol. 4, no. 2, pp. 35–51, 1992.

[9] C. T. Ewing, F. R. Faith, J. T. Hughes, and H. W. Carhart, "Flame extinguishment properties of dry chemicals: extinction concentrations for small diffusion pan fires," *Fire Technology*, vol. 25, no. 2, pp. 134–149, 1989.

[10] Z. Jiang, W. K. Chow, and S. F. Li, "Review on additives for new clean fire suppressants," *Environmental Engineering Science*, vol. 24, no. 5, pp. 663–674, 2007.

[11] Y. Yan, Z. Han, L. Zhao, Z. Du, and X. Cong, "Study on the relationship between the particle size distribution and the effectiveness of the K-powder fire extinguishing agent," *Fire and Materials*, vol. 42, no. 3, pp. 336–344, 2018.

[12] J. Zhao, Z. Yin, M. Usman Shahid et al., "Superhydrophobic and oleophobic ultra-fine dry chemical agent with higher chemical activity and longer fire-protection," *Journal of Hazardous Materials*, vol. 380, Article ID 120625, 2019.

[13] D. G. Elliott, P. W. Garrison, G. A. Klein, K. M. Moran, and M. P. Zydowicz, *Flow of Nitrogen-Pressurized Halon 1301 in Fire Extinguishing Systems*, Jet propulsion labartorty, California, USA, 1984.

[14] T. G. Cleary, W. L. Grosshandler, and J. C. Yang, *Flow of Alternative Agents in Piping*, National Institute of Standards and Technology, Maryland, U.S.A, 1995.

[15] T. G. Cleary, J. C. Yang, M. D. King, C. I. Boyer, and W. L. Grosshandler, "Pipe flow characteristics of alternative agents for engine nacelle fire protection," *Proceedings on Halon Options Technical Working (lmferek~ May*, vol. 9, p. 11, 1995.

[16] Z. B. Tong, B. Zheng, R. Y. Yang, A. B. Yu, and H. K. Chan, "CFD-DEM investigation of the dispersion mechanisms in commercial dry powder inhalers," *Powder Technology*, vol. 240, pp. 19–24, 2013.

[17] J. Yang, C.-Y. Wu, and M. Adams, "DEM analysis of particle adhesion during powder mixing for dry powder inhaler formulation development," *Granular Matter*, vol. 15, no. 4, pp. 417–426, 2013.

[18] J. Yang, C.-Y. Wu, and M. Adams, "Three-dimensional DEM-CFD analysis of air-flow-induced detachment of API particles from carrier particles in dry powder inhalers," *Acta Pharmaceutica Sinica B*, vol. 4, no. 1, pp. 52–59, 2014.

[19] J. Yang, C. Y. Wu, and M. Adams, "DEM analysis of the effect of particle–wall impact on the dispersion performance in carrier-based dry powder inhalers," *International Journal of Pharmaceutics*, vol. 487, no. 1-2, pp. 32–38, 2015.

[20] Z. Tong, W. Zhong, A. Yu, H.-K. Chan, and R. Yang, "CFD-DEM investigation of the effect of agglomerate-agglomerate collision on dry powder aerosolisation," *Journal of Aerosol Science*, vol. 92, pp. 109–121, 2016.

[21] M. Ariane, M. Sommerfeld, and A. Alexiadis, "Wall collision and drug-carrier detachment in dry powder inhalers: using DEM to devise a sub-scale model for CFD calculations," *Powder Technology*, vol. 334, pp. 65–75, 2018.

[22] R. Ponzini, R. Da Vià, S. Bnà, C. Cottini, and A. Benassi, "Coupled CFD-DEM model for dry powder inhalers simulation: validation and sensitivity analysis for the main model parameters," *Powder Technology*, vol. 385, 2021.

[23] S. Peng, Q. Chen, C. Shan, and D. Wang, "Numerical analysis of particle erosion in the rectifying plate system during shale gas extraction," *Energy Science & Engineering*, vol. 7, no. 5, pp. 1838–1851, 2019.

[24] E. Liu, D. Li, W. Li et al., "Erosion simulation and improvement scheme of separator blowdown system --A case study of Changning national shale gas demonstration area," *Journal of Natural Gas Science and Engineering*, vol. 88, Article ID 103856, 2021.

[25] S. Peng, Q. Chen, C. Zheng, and E. Liu, "Analysis of particle deposition in a new-type rectifying plate system during shale gas extraction," *Energy Science & Engineering*, vol. 8, no. 3, pp. 702–717, 2020.

[26] D. A. Drew and R. T. Lahey, *Particulate Two-phase Flow*-Butterworth-Heinemann, Boston, 1993.

[27] D. Gidaspow, R. Bezburuah, and J. Ding, *Hydrodynamics of Circulating Fluidized Beds: Kinetic Theory Approach (No. CONF-920502-1)*, Illinois Inst. of Tech., Chicago, IL, USA, 1991, https://www.osti.gov/servlets/purl/5896246.

[28] C. Y. Wen, "Mechanics of fluidization," *Chemical Engineering Progress Symposium Series*, vol. 62, pp. 100–111, 1966.

[29] S. Ergun, "Fluid flow through packed columns," *Chemical Engineering Progress*, vol. 48, pp. 89–94, 1952.

[30] C. K. K. Lun, S. B. Savage, D. J. Jeffrey, and N. Chepurniy, "Kinetic theories for granular flow: inelastic particles in Couette flow and slightly inelastic particles in a general flowfield," *Journal of Fluid Mechanics*, vol. 140, pp. 223–256, 1984.

[31] D. Gidaspow, *Multiphase Flow and Fluidization: Continuum and Kinetic Theory Descriptions*, Academic Press, Cambridge, Massachusetts, 1994.

[32] M. Syamlal, W. Rogers, and T. J. OBrien, "MFIX Documentation Theory Guide," USDOE Morgantown Energy Technology Center, WV USA, 1993, https://www.osti.gov/servlets/purl/10145548.

[33] D. G. Schaeffer, "Instability in the evolution equations describing incompressible granular flow," *Journal of Differential Equations*, vol. 66, no. 1, pp. 19–50, 1987.

[34] F. R. Menter, "Two-equation eddy-viscosity turbulence models for engineering applications," *AIAA Journal*, vol. 32, no. 8, pp. 1598–1605, 1994.

[35] J. O. Hinze, *Turbulence*, McGraw-Hill Publishing Co, NY, USA, 1975.
[36] Y. W. Cai, *Simulation of Flow Resistance in Horizontal Straight Pipe of Superfine Dry Powder Extinguishing Agent*, Nanjing University of Science and Technology, China, 2014.